Polymer Vol. 38 No. 10, pp. 2299–2305, 1997

0032-3861/97/$17.00 + 0.00

PII: S0032-3861(96)00788-4

polymer papers

Study of holographic gratings in poly(methyl-2-cyanoacrylate) by neutron diffraction

R. A. Rupp*, U. Hellwig and U. Schellhorn
Fachbereich Physik der Universität Osnabrück, D-49069 Osnabrück, Germany

and J. Kohlbrecher and A. Wiedenmann
Hahn-Meitner-Institut, D-14109 Berlin, Germany

and J. Woods
LOCTITE Corporation, Newington, CT 06111, USA
(Received 8 March 1996; revised 3 June 1996)

Using a holographic two-beam set-up, thick refractive-index gratings are recorded in photopolymers based on poly(methyl-2-cyanoacrylate). We demonstrate diffraction of cold neutrons from these gratings, a property reported hitherto only for photopolymer systems based on poly(methyl methacrylate). Applying both methods, neutron and light diffraction experiments, we have succeeded in separating the contributions of the light-induced density and refractivity modulations to the change in light-optical refractive index. © 1997 Elsevier Science Ltd.

(Keywords: photopolymers; holographic recording; neutron diffraction; relaxation)

INTRODUCTION

Interest in holographic recording materials has grown in the last years, in particular in those suitable for recording volume phase holograms. Photopolymers have been found to be very attractive for holographic storage and production of holographic optical elements because of their high sensitivity, ease of preparation and self-development capability[1].

One of the most intensively investigated photopolymer systems for optical storage is based on poly(methyl methacrylate) (PMMA)[2,3]. The photochemical mechanism of the formation of the refractive index pattern in PMMA is due to photopolymerization of residual monomers giving rise to a photoinduced diffusive mass transport. This results in a mass density modulation which contributes not only to a modulation of the light-optical refractive index but also of the neutron-optical refractive index. As a consequence, holographically written gratings diffract neutrons similarly to light[4,5].

Another family of organic materials for holographic storage comprises the poly(alkyl-2-cyanoacrylates)[6–10]. The chemical formulae of the monomer methyl-2-cyanoacrylate (MCA) and of the polymer poly(methyl-2-cyanoacrylate) (PMCA) are shown in *Figure 1*. The very reactive MCA is a well-known basic component of commercial adhesives. The monomer is usually polymerized by an anionic mechanism, but free radical polymerization is also possible[11]. Polymerization starts, for example, when alkyl-2-cyanoacrylate is placed between glass plates with small amounts of water or other bases present on the surfaces. The scheme of the chemical reaction is discussed in refs 12 and 13.

The photorefractive mechanism of PMCA is still under debate. Either it is assumed to result from chain scission or—as for PMMA—from photopolymerization of residual monomers. Pinsl *et al.*[14] give two reasons in favour of the latter model: (1) holograms in poly(alkyl-2-cyanoacrylates) continue to grow in the dark, which indicates continuing chain growth by monomer diffusion; (2) they found a discrepancy between the measured refractive index change and the one calculated from the observed absorption changes using the Kramers–Kronig relation. Both arguments are rather indirect and, in the latter case one might object that only a small part of the absorption spectrum was evaluated. While a mass density modulation should be negligible in the case of the other model, the photorefractive mechanism proposed by Pinsl *et al.* necessarily implies a strong density modulation. It is therefore possible to decide between the above models by neutron diffraction experiments, as they provide information on the light-induced density structures which, on principle, cannot be solely obtained from light diffraction.

Another motivation for this work is a general interest in new materials with improved characteristics for neutron diffraction from light-induced structures. It is fed by the attractive perspective that neutron optical devices could be produced by light-optical means. As we would thereby profit from the high standard of light-optical technology, any arbitrary refractive index pattern could be produced by choosing suitable wave fields during hologram recording.

* To whom correspondence should be addressed

Figure 1 Methyl-2-cyanoacrylate and poly(methyl-2-cyanoacrylate)

THEORY

Wherever it is necessary to distinguish between quantities referring to light or neutrons in the following, we will label them with an index L or N, respectively, and quantities referring to monomers and polymers with an index m or p, respectively.

Holographic recording

In our model we consider a polymer matrix playing the role of a sponge and some residual monomers filling it. Initially the total polymer system is homogeneous. The number density of bound monomeric units (monomers in a polymer chain) is then defined by $N_p = w_p\rho/M$, where ρ is the density of the total polymer system, $w_p = m_p/(m_p + m_m)$ the mass fraction of polymer, m_m and m_p are the masses of the monomer and the polymer portions, respectively, and M is the molecular mass. The number density of free, i.e. mobile residual monomers can be defined analogously.

Assuming linear response of the photorefractive medium, the sinusoidal interference pattern of two coherent plane light waves

$$I(0)(1 + m\cos \boldsymbol{K}\cdot\boldsymbol{r}) \tag{1}$$

acting on the medium generates a change

$$\delta N_p(0) + \delta N_p(K)\cos(\boldsymbol{K}\cdot\boldsymbol{r} + \phi) \tag{2}$$

of the polymer density. Here $I(0)$ is the average intensity, m the modulation degree, $\boldsymbol{K}$ the grating vector, $|\boldsymbol{K}| = 2\pi/\Lambda$ the spatial frequency, $\Lambda = \lambda_L/2n_L \sin\theta_B$ the period of the grating, λ_L the wavelength of light in vacuum, n_L the refractive index for light, θ_B the half-angle (Bragg angle within the medium) between the propagation directions of both waves, and ϕ accounts for a possible phase shift between refractive index and light intensity pattern. In the linear recording range assumed here we have $\delta N_p(K) = g(K)I(K)$, where $I(K)$ is the Fourier component of the light intensity with spatial frequency K and $g(K)$ the response of the medium.

The pertinent complementary change of the number density of the residual monomers is given by

$$\delta N_m(0) + \delta N_m(K)\cos(\boldsymbol{K}\cdot\boldsymbol{r} + \phi) = -[\delta N_p(0) + \delta N_p(K)\cos(\boldsymbol{K}\cdot\boldsymbol{r} + \phi)] \tag{3}$$

As the density of the monomer is lower than that of the polymer[11], the effective volume occupied by a monomer is larger than the one occupied by a monomer unit of the chain, which means that photopolymerization increases the free volume in the illuminated areas. This triggers relaxation processes. Provided that the sample contains sufficient residual monomers, diffusion will be dominated by residual monomers, because their mobility is larger than that of the polymer chains. The diffusion processes tend to fill up the free volume and average out the spatial modulation N_m of the monomer density. The final result is a modulation of the density ρ and hence of the total number density $N = \rho/M = N_m + N_p$:

$$\delta N(0) + \delta N(K)\cos(\boldsymbol{K}\cdot\boldsymbol{r} + \phi), \tag{4}$$

where $\delta N(0)$ is the change of the average density, $\delta N(K)$ the amplitude of the modulated number density.

We assume that the relation between the light-optical refractive index and the total density $N = N_m + N_p$ can be described by the Lorentz–Lorenz relation:

$$\frac{n_L^2 - 1}{n_L^2 + 2} = N\bar{R} \tag{5}$$

The average refractivity of the polymer is given by

$$\bar{R} = (1 - w_p)R_m + w_pR_p \tag{6}$$

where R_m and R_p are refractivities of the monomer and the polymer, respectively.

Photopolymerization induces a change

$$\delta n_L(K) = \frac{(n_L^2 + 2)^2}{6n_L}[R_m\delta N_m(K) + R_p\delta N_p(K)] \tag{7}$$

of the refractive index for light.

For cold neutrons there is no difference between free monomers and monomers bound in a polymer chain; i.e., we would have $R_m = R_p$ for a quantity analogous to the refractivity. Therefore the amplitude of the refractive index change for neutrons is simply proportional to the number density change $\delta N = \delta N_m + \delta N_p$ and is given by

$$\delta n_N(K) \approx \frac{\lambda_N^2}{2\pi} b\delta N(K) \tag{8}$$

Here b denotes the coherent scattering length of a monomer unit and λ_N the neutron wavelength.

Diffraction

Plane wave diffraction of light from thick gratings is described by the coupled-wave theory[15] and of neutrons by the dynamical diffraction theory[16]. For the Laue case the diffraction efficiency is given by

$$\eta = T\nu^2 \frac{\sin^2\sqrt{\nu^2 + \xi^2}}{\nu^2 + \xi^2} \tag{9}$$

The parameter $\nu = \pi d\delta n/\lambda\cos\theta_B$ measures the strength of the grating and $\xi = \pi\Delta\theta d/\Lambda$ the deviation from the Bragg angle, where d is the thickness of the grating and $\Delta\theta$ is the difference between Bragg angle and angle of incidence within the medium. Depending on the type of radiation considered, the appropriate light-optical or neutron-optical material constants have to be substituted for the refractive index n and its change δn as well as for the extinction constant α. Note that only ν and the transmission $T = \exp(-\alpha d/\cos\theta)$ depend on these material constants and on the wavelength, but not the parameter ξ. This is the reason for the similarity of

light-optical and neutron-optical rocking curves, i.e. curves obtained by recording the diffraction efficiency as a function of the angle of incidence. Internal angles θ have to be calculated from the measured external angles ω with the appropriate average refractive index $n_L \approx 1.5$ for light and $n_N \approx 1.0$ for neutrons. The maximum diffraction efficiency

$$\eta(0) = T \sin^2 \nu \tag{10}$$

is found for exact Bragg incidence, i.e. for $\xi = 0$.

As mentioned above, the equation for the diffraction efficiency is only valid for coherent plane waves. Neutron diffraction experiments are, however, always performed with more or less incoherent sources, which leads to a smearing out of the rocking curves; i.e., the rocking curves are convoluted with the spatial frequency and wavelength spectra of the source. Typically, we work at small angle neutron scattering (SANS) facilities with a beam divergence of about $\Delta\omega \approx 1$ mrad and a wavelength distribution of $\Delta\lambda_N/\lambda_N \approx 10\%$. Though the latter seems to be large, its effect corresponds only to an equivalent angle of divergence of the order of 0.1 mrad; i.e., the effect of temporal incoherence is usually negligible in comparison with the effect of lateral incoherence. Let us therefore postpone the problem of the small correction for the effect of wavelength distribution.

A possible way to evaluate the data is to calculate the convolution over the angular distribution function. This procedure is rather cumbersome, because additional information on the beam properties of the neutron scattering instrument is required. As we are only interested in the parameter ν, which contains all information on the light-induced density change $\delta N(K)$, there is a much easier way, namely to calculate the *integral diffraction efficiency* (integrated reflectivity)

$$\bar{\eta} = \int \eta \mathrm{d}\xi = \frac{\pi d}{\Lambda} \int \eta \mathrm{d}\theta \approx \pi\eta(0) \tag{11}$$

from the data, which is the diffraction efficiency integrated over the whole rocking curve. The advantage is that the integral diffraction efficiency no longer depends on the lateral coherence properties of the instrument. The relative error of the approximation on the right-hand side of the above equation is less than 7×10^{-3} for values up to $\nu = 1$.

As in our case the integral diffraction efficiency for neutrons remains smaller than 10^{-2}, we use the approximations

$$\eta_N(0) \approx T_N \left(\frac{1}{2}\lambda_N b d \delta N(K)\right)^2 \tag{12}$$

and

$$\frac{\bar{\eta}}{\pi} = \frac{d}{\Lambda} \int \eta \mathrm{d}\theta = T_N[1 + h]\left(\frac{1}{2}\lambda_N b d\ \delta\ N(K)\right)^2 \tag{13}$$

The transmission factor $T_N = \exp(-\alpha_N d)$ accounts for elastic, inelastic and incoherent neutron scattering loss processes and absorption; i.e., $\sigma_T = \alpha_N/N$ is the total scattering cross-section.

In the last expression we have included a usually negligible correction $h = (1/6)(\Delta\lambda_N/\lambda_N)^2$ which accounts for averaging over the wavelength distribution. Thereby we have assumed a triangular distribution with central wavelength λ_N and relative half-width $\Delta\lambda_N/\lambda_N$, an assumption which is appropriate for the velocity selector of the SANS instrument V4 at the Hahn-Meitner-Institut Berlin[17].

Perhaps we should note, finally, that the density modulation calculated from equation (12) means the r.m.s. value in inhomogeneous gratings and that, using the value of ν evaluated by the procedure just described, we could in principle deduce the beam properties of the instrument by fitting the rocking curves to the angular distribution functions.

EXPERIMENTAL

Methyl-2-cyanoacrylate monomer (MCA), containing a small amount of anionic polymerization inhibitor, was received from Loctite Corporation and used without further purification. The u.v. and visible light sensitive photoanionic initiator, potassium reineckate, having the chemical structure $K[Cr(NH_3)_2(NCS)_4]$, was prepared under dim red light conditions according to the literature procedure[18]; this material has previously been shown to be an efficient photoinitiator of cyanoacrylate polymerization[19]. We prepared solutions of MCA with photoinitiator concentrations between 200 and 375 ppm. The solution was poured into a small cuvette consisting of two 1 mm thick glass slides and a spacer. The spacer was a flexible PVC tube, permitting compensation for the volume contraction during polymerization. Polymerization was initiated by squeezing the cuvette. Typically we obtained solid polymer blocks with an area of $2 \times 2\,\mathrm{cm}^2$ and a thickness of about 1 mm.

Gratings with grating periods between 200 nm and 2 μm were written at the wavelength $\lambda = 351.1$ nm of an Ar^+ ion laser using a conventional two-beam interference set-up in symmetrical arrangement. The laser beams were expanded in order to illuminate the whole area of the sample nearly homogeneously. During recording the sample remained in the cuvette and was exposed for 60 s with a total intensity of about $350\,\mathrm{W\,m^{-2}}$.

The grating periods of the samples were determined by light diffraction with $\lambda_L = 488$ nm or 351 nm. To that purpose the angle $2\theta_B$ between the +1st and −1st order peaks was measured and the grating period was calculated from Bragg's condition.

The experiments with neutrons were carried out on the SANS instrument V4 at the research reactor of the Hahn-Meitner-Institut in Berlin. We used a beam of cold neutrons ($\lambda_N = 1.4$ nm) with a collimation length of 16 m, corresponding to a divergence of 1.8 mrad. The samples were placed behind a cadmium diaphragm on a rotary table. The neutrons were counted by a conventional two-dimensional multidetector at a sample–detector distance of 16 m.

Transmission measurements were made for some PMCA samples at several (central) wavelengths between 0.5 nm and 2 nm. For the diffraction experiments the samples were mounted on a rotation stage with its ω axis vertical to the plane of incidence. The rotation angle ω between the beam axis and the normal to the sample surface was varied between −5.5 mrad and +5.5 mrad in steps of 0.25 mrad. The grating vector $\boldsymbol{K}$ was in the plane of incidence, nearly perpendicular to the neutron beam. In order to obtain a sufficient neutron count rate with a statistical error of less than 1% for a wavelength distribution of $\Delta\lambda_N/\lambda_N = 9\%$ (at $\lambda_N = 1.4$ nm), an acquisition time of about 15–20 min for each angular setting was chosen.

RESULTS

The samples were investigated by optical diffraction measurements. The main characteristics of some representative gratings are summarized in *Table 1*. *Figures 2* and *3* show the diffraction for the first-order peak of samples 2 and 5 with grating periods $\Lambda_L = (276 \pm 4)$ nm and $\Lambda_L = (2.05 \pm 0.02)\,\mu$m, respectively.

Samples 1, 2 and 3 were also investigated by neutron diffraction experiments. As an example, *Figure 4* shows the essential part of the detector matrix with the neutron scattering pattern of sample 2 at the angle of incidence $\omega = +2.51$ mrad, which is the angle of the +1st order of Bragg diffraction. We recognize a well-resolved Bragg peak on the right side of the primary beam which is blocked by a beam stop. A similar peak occurs on the left side of the primary beam for the angle of incidence $\omega = -2.51$ mrad of the −1st Bragg order (not shown in the figure). Both Bragg peaks appear at the detector elements corresponding to the angle of emergence expected from the spacial frequency $K = 2\pi/\Lambda \approx 23\,\mu m^{-1}$. They disappear on violation of the Bragg condition, i.e. for $\omega \neq \pm 2.51$ mrad. The angular difference between the peak positions (see *Figure 5*) agrees, within the error margins, with the grating spacing of $\Lambda = 276$ nm.

The rocking curve of sample 2, i.e. its diffraction efficiency as a function of the angle of incidence ω, is shown in *Figure 5* for $\lambda_N = 1.4$ nm. The data are corrected for detector sensitivity, signal noise and background. The positions of both maxima correspond to the ±1st order diffractions of a grating with 278 nm ± 6 nm periodicity in accordance with the result of light diffraction measurements. The peak efficiency reaches 0.1%, but the heights of the ±1st Bragg peaks differ by about 20% for reasons not yet understood.

The 1.3 mm thick sample 2 has a transmission of approximately 44% for neutrons with a wavelength of 14 Å. We carried out a series of transmission measurements on several PMCA samples with and without the grating as a function of the neutron wavelength varying between 0.5 nm and 2 nm. The first two columns of *Table 2* summarize the results.

Table 1 Results of light-optical diffraction measurements (d = thickness of the sample; Λ_L = grating period determined by light diffraction; $\eta_L(0)$ = efficiency of light diffraction measured at λ_L = 488 nm (except for sample 1, where λ_L = 351.1 nm); δn_L = amplitude of the index of refraction)

Sample	d (mm)	Λ_L (nm)	$\eta_L(0)$ (%)	δn_L
1	1.2	206	28	0.5×10^{-4}
2	1.3	276	77	1.0×10^{-4}
3	1.3	276	57	0.8×10^{-4}
4	1.4	353	11	0.3×10^{-4}
5	1.2	2050	94	1.7×10^{-4}

DISCUSSION

Light diffraction

Unlike previous work (e.g. ref. 14), we induce holographic gratings in PMCA by anionic photopolymerization and reach diffraction efficiencies of nearly 30% at grating spacings of about 200 nm, nearly 80% at about 300 nm and more than 90% at about 2 μm. Therefore PMCA can be considered as a holographic recording material of high efficiency as well as high resolution. The maximum refractive index changes are 10×10^{-5} at 276 nm, practically the same as found for PMMA, where we measured for example, 8×10^{-5} at 350 nm. The examples given in the table indicate, however, that the procedure by which photosensitive samples are produced may lead to results which scatter up to 50% in terms of refractive index change.

Similar to PMMA, we observe well-resolved side lobes in the rocking curves for large grating spacings (*Figure 3*), as expected from equation (9). The angular difference between two side lobes corresponds to the sample thickness. However, there is nearly no structure around the Bragg angle for small grating spacings (*Figure 2*). The curves are much broader than those predicted by the theory for ideal gratings. As for PMMA, we assume that these features come from grating distortions and inhomogeneities in the sample which lead to a dephasing in the diffracted wave field.

Neutron diffraction

The most prominent result of our investigation is that photoinduced gratings recorded in PMCA exhibit rather

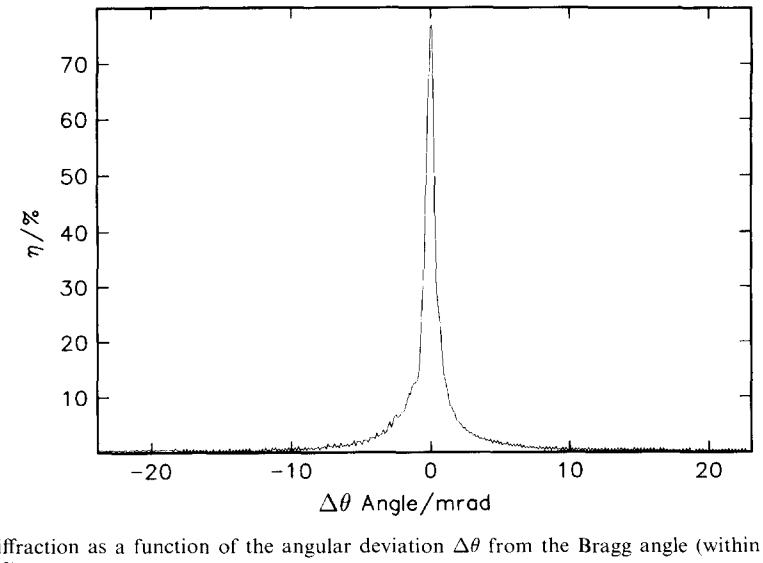

Figure 2 Efficiency of light diffraction as a function of the angular deviation $\Delta\theta$ from the Bragg angle (within the medium) for a grating with $\Lambda = 276$ nm in PMCA (sample 2)

strong neutron diffraction, regarding the fact that the polymer is not deuterated. The maximum efficiency for PMCA at $\lambda_N = 1.4\,nm$ is 0.5‰, whereas we find under similar conditions only 0.2‰ for PMMA[5]. Thus PMCA is not only the second photopolymer system found to exhibit a photorefractive effect for neutrons, but also the more interesting one in view of possible neutron-optical devices and applications.

Three reasons can be put forward to explain the comparatively large neutron diffraction efficiencies of PMCA. The first one is the large coherent scattering length of the monomers which enters the diffraction efficiency quadratically. For the long wavelengths used in our experiments, the coherent scattering length $b = \Sigma_i b_i$ of the monomer molecule is simply the sum of the coherent scattering lengths b_i of all pertinent nuclei labelled here by the index i. Using data of ref. 20 for the nuclei we obtain $b = 14.92\,fm$ for methyl methacrylate (MMA), but $b = 35.50\,fm$ for MCA, because three protons of one of the methyl groups of MMA are replaced in MCA by a nitrogen nucleus which has a large positive scattering length. The second reason is the lower incoherent scattering cross-section σ_i. Its value is $\sigma_i = 402 \times 10^{-28}\,m^2$ for MCA, but $\sigma_i = 642 \times 10^{-28}\,m^2$ for MMA, which results in a higher transmission T_N of PMCA—at least theoretically. The third one is the fact that an appreciable density modulation exists in PMCA.

In order to deduce the density amplitude $\delta N(K)$ from the data we calculate the integrated diffraction efficiency $\bar{\eta}$ and evaluate from it the diffraction efficiency in the coherency limit, $\eta_N(0)/T_N \approx 0.9\%$. Temporal incoherence changes this value only in the range of some 10^{-3}, which is negligible.

The grating spacings Λ_N calculated from the results of neutron diffraction experiments (*Table 3*) are systematically somewhat larger than those determined from light diffraction experiments. The possible origin may be a systematic error of about 2% in the calibration of the monochromator of the SANS instrument, since the neutron wavelength is nowhere near as precisely determined as the laser wavelength. In the same way the relative errors (~3%) for the grating spacings Λ_N from the neutron experimental data (right column in *Table 3*) are smaller than the relative wavelength distribution $\Delta\lambda_N/\lambda_N = 9\%$. They are determined rather by the accuracy of the central wavelength λ_N itself than by its shift ($< [\Delta\lambda_N/\lambda_N]^2$) owing to the quadratic wavelength dependence of the diffraction efficiency (see equation (12)).

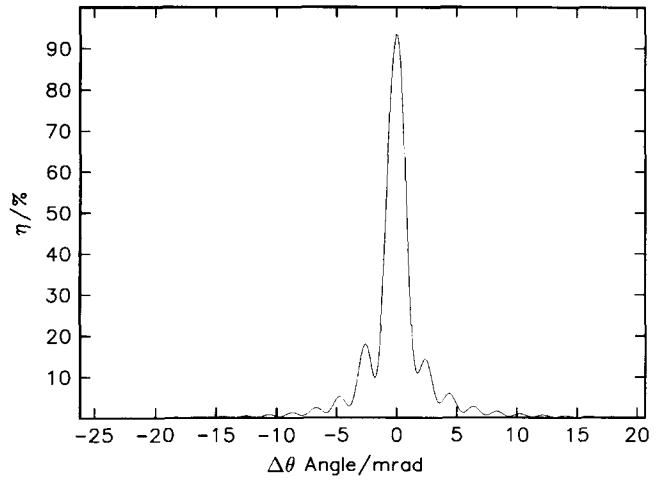

Figure 3 Efficiency of light diffraction as a function of the angular deviation $\Delta\theta$ from the Bragg angle (within the medium) for a grating with $\Lambda = 2.05\,\mu m$ in PMCA (sample 5)

Photorefractive mechanism

Without any doubt, the gratings from which neutrons and light are diffracted have the same origin, because the grating spacings determined by light and neutron diffraction agree within the error margins (*Table 3*). The fact that there is neutron diffraction is a clear proof of the existence of a density grating. With the value $\eta_N(0)/T_N \approx 0.9\%$ we obtain a modulation amplitude of

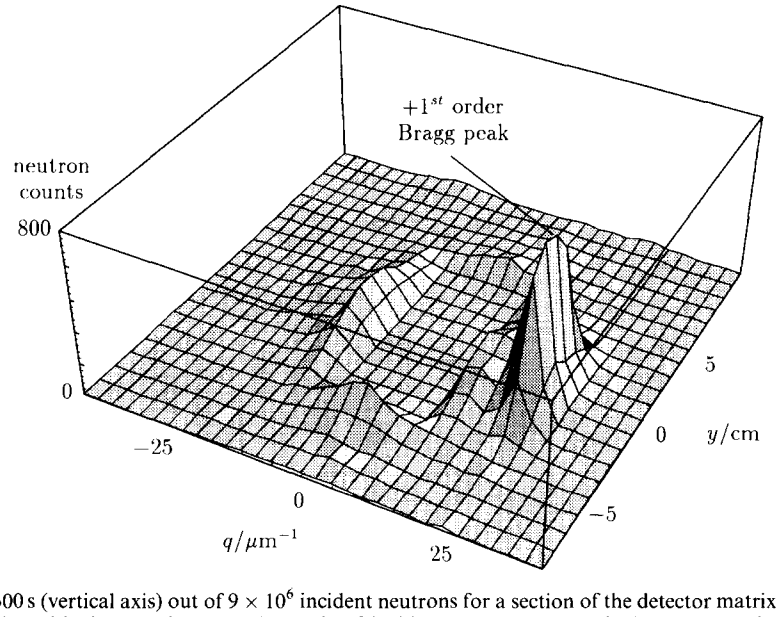

Figure 4 Neutron counts in 1300 s (vertical axis) out of 9×10^6 incident neutrons for a section of the detector matrix around the suppressed primary beam in a three-dimensional plot with the sample set at the angle of incidence $\omega = +2.51$ mrad; the Bragg peak occurs on the right side of the suppressed primary beam ($\lambda_N = 1.4\,nm$, angular beam divergence $\Delta\omega = 1.8$ mrad, $\Delta\lambda_N/\lambda_N = 9\%$, sample–detector distance $s = 16\,m$, size of detector elements $\Delta x = \Delta y = 1\,cm$). The horizontal x-axis of the detector was converted to momentum transfer $q = 2\pi x/s\lambda_N$

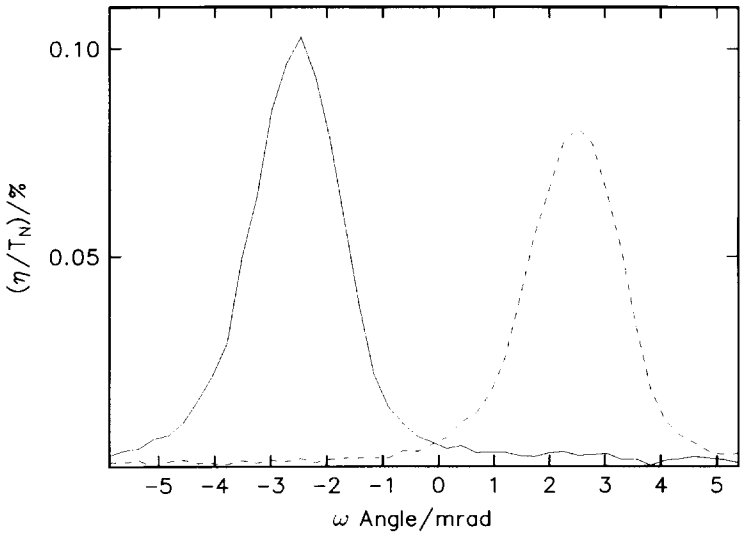

Figure 5 Neutron diffraction efficiency divided by sample transmission vs angle of incidence ω for sample 2 (optically determined grating period: $\Lambda = 276\,\text{nm} \pm 4\,\text{nm}$) for cold neutrons ($\lambda_N = 1.4\,\text{nm}$, $\Delta\omega = 1.8\,\text{mrad}$, $\Delta\lambda_N/\lambda_N = 9\%$). The full line denotes the diffraction efficiency for the +1st order peak and the broken line that for the −1st order peak. The neutron diffraction efficiency was corrected for the scattering count rates at large Bragg mismatch, for the sensitivity of the detector matrix, background noise and transmission

Table 2 Neutron transmission measurements at room temperature (λ_N = neutron wavelength; σ_T = measured total scattering cross-section; σ_a = calculated absorption cross-section; σ_i = calculated incoherent scattering cross-section; $\Delta\sigma$ = difference between the measured total cross-section and the latter two contributions)

λ_N (nm)	σ_T (barn)	σ_a (barn)	σ_i (barn)	$\Delta\sigma$ (barn)
0.5	497	10	402	85
1.0	737	20	402	315
1.4	898	28	402	468
2.0	1128	40	402	686

Table 3 Comparison of grating periods measured by light diffraction (Λ_L) and neutron diffraction (Λ_N)

Sample	Λ_L (nm)	Λ_N (nm)
1	(206 ± 4)	(216 ± 6)
2	(276 ± 4)	(278 ± 6)
3	(276 ± 4)	(280 ± 6)

the neutron refractive index of $\delta n_N = 3.5 \times 10^{-8}$ at $\lambda_N = 1.4\,\text{nm}$ and a density amplitude of

$$\delta N(K) = \delta N_m(K) + \delta N_p(K) = 3 \times 10^{24}\,\text{m}^{-3} \quad (14)$$

From equation (9) we obtain $\delta n_L = 1.0 \times 10^{-4}$ and from equation (7) we calculate

$$R_m \delta N_m(K) + R_p \delta N_p(K) = 6 n_L \delta n_L/(n_L^2 + 2)^2 = 5.0 \times 10^{-5} \quad (15)$$

From the refractive indices $n_m = 1.443$ and $n_p = 1.50$, the densities $\rho_m = 1.1\,\text{g cm}^{-3}$ and $\rho_p = 1.3\,\text{g cm}^{-3}$ of the monomer and the polymer[11], and the molecular mass $M = 111\,\text{g}$, we deduce the values $R_m = 4.5 \times 10^{-29}\,\text{m}^3$ and $R_p = 4.2 \times 10^{-29}\,\text{m}^3$ for the monomer and polymer refractivities. Then we obtain finally, from equations 14 and 15, the absolute values of the density modulations: $\delta N_p(K) = 2.8 \times 10^{25}\,\text{m}^{-3}$ and $\delta N_m(K) = -2.5 \times 10^{25}\,\text{m}^{-3}$ for $K = 23\,\mu\text{m}^{-1}$.

We can cross-check this result by a reasoning based on the free volume hypothesis. If polymer diffusion can be neglected, the density amplitude $\delta N_p(K)$ arises only due to photopolymerization of monomers and creates a modulation of the free volume $\delta V_f/V = 7.6 \times 10^{-4}$, where V_f is the free volume and V the unit volume. As the volume occupied by one MCA molecule is $1.7 \times 10^{-28}\,\text{m}^3$, the maximum number density of MCA molecules which can be fitted into this free volume is $\delta N_{max} = 4.5 \times 10^{24}\,\text{m}^{-3}$. Comparing this with equation (14), we find that the free volume generated by the photopolymerization process is occupied, with $\delta N/\delta N_{max} = 75\%$, by monomers. As many quantities in our estimation are not determined with the precision required, there may be an error of approximately 20%, i.e. the fraction of the free volume occupied by diffusion of free monomers is between 55% and 95%.

Nevertheless, by using the results of light and neutron diffraction, we have obtained a satisfying, consistent picture of the photorefractive mechanism. Initially, photopolymerization generates an antiphase modulation of the polymer and the monomer density $\delta N_p = -\delta N_m = 3.0 \times 10^{25}\,\text{m}^{-3}$. At the same time there is a free volume modulation $\delta V_f/V = 2.6 \times 10^{-10}$, because the volume occupied by a monomer unit in the polymer chain is about 17% smaller than the one occupied by a residual monomer. At this time there should be no neutron diffraction as the total density δN is zero and the initial refractive index amplitude, totally determined by the refractivity change, should be $\delta n_{L,R} = -1.8 \times 10^{-4}$. Subsequently, relaxation processes set in. We assume that they are dominated by diffusion of residual monomers. They essentially fill up the light-induced free volume and generate an excess modulation amplitude $\delta N(K) = 3 \times 10^{24}\,\text{m}^{-3}$ of the density measured by neutron diffraction. The pertinent density-determined contribution to the refractive index change is $\delta n_{L,N} = +2.7 \times 10^{-4}$. Both contributions add up to the refractive index change $\delta n_L = 1.0 \times 10^{-4}$, measured by light diffraction.

Neutron transmission

Total scattering cross-sections σ_T per monomer unit, determined for cold neutrons in the range between 0.5 nm and 2 nm, are given in *Table 2* together with

absorption and incoherent scattering cross-sections using data from ref. 20. If we subtract the latter contributions from σ_T we obtain a residual contribution $\Delta\sigma$ which cannot be explained by the small amounts of inhibitors and photoinitiator present in the sample. The residual contribution increases linearly with increasing neutron wavelength and may arise either from coherent scattering induced by noisy density structures in the polymer, from inelastic scattering[21,22], or from both.

CONCLUSIONS

Our experiments demonstrate the possibility of producing photoinduced gratings in PMCA with grating periods down to 200 nm by anionic photopolymerization. Diffraction of cold neutrons from these gratings, reported here for the first time, clearly proves the existence of a density grating and is the key for an understanding of the photorefractive mechanism. The final density modulation results from two steps. First, illumination causes repolymerization of residual monomers which induces a light-optical refractive index grating due to the difference in refractivities as well as a free-volume grating. The second step consists of a relaxation process in which the monomers occupy the free volume by diffusion, thus creating a density grating. The first step, i.e. the generation of a light-optical refractive index grating without a simultaneous density grating, is still a hypothesis which has to be checked in future experiments. In order to check the model further it is highly desirable to find out whether the light and neutron refractive index gratings follow the same relaxation dynamics.

The process in PMCA seems to be similar to the one in PMMA, as does the order of magnitude of the process. However, the neutron optical material constants, i.e. the coherent scattering length per molecule and the total cross-section for losses, are better, which makes PMCA a promising material for future applications in neutron optics.

ACKNOWLEDGEMENT

Financial support by the BMBF (project RU11.12K) is gratefully acknowledged.

REFERENCES.

1. Tomlinson, W. J. and Chandross, E. A., *Adv. Photochem.* 1980, **12**, 201.
2. Kopietz, M., Lechner, M. D., Steinmeier, D. G. and Franke, H., *Makromol. Chem.* 1986, **187**, 2787.
3. Franke, H., Festl, H. G. and Krätzig, E., *Colloid. & Polym. Sci.* 1984, **262**, 213.
4. Rupp, R. A., Hehmann, J., Matull, R. and Ibel, K., *Phys. Rev. Lett.* 1990, **64**, 301.
5. Matull, R., Rupp, R. A., Hehmann, J. and Ibel, K., *Zeitschr. Phys. B—Condensed Matter* 1990, **81**, 365.
6. Bräuchle, C., Wild, U. P., Burland, D. M., Bjorklund, G. C. and Alvarez, D. C., *IBM J. Res. Dev.* 1982, **26**, 217.
7. Bräuchle, C., Wild, U. P., Burland, D. M., Bjorklund, G. C. and Alvarez, D. C., *Optic. Letts.* 1982, **7**, 177.
8. Gerbig, V., Grygier, R. K., Burland, D. M. and Sincerbox, G., *Optic. Letts.* 1983, **8**, 404.
9. Pinsl, J., Gehrtz, M., Reggel, A. and Bräuchle, C., *J. Am. Chem. Soc.* 1987, **109**, 6479.
10. Friesem, A. A., Rav-Noy, Z. and Reich, S., *Appl. Optics* 1977, **16**, 427.
11. Canale, A. J., Goode, W. E., Kinsinger, J. B., Panchak, J. R., Panchak, R. L., Kelso, R. L. and Graham, R. K., *J. Appl. Polym. Sci.* 1960, **4**, 231.
12. Coover, H. W., Jr, Joyner, F. B., Shearer, N. H., Jr and Wickler, T. H., Jr *Society of Plastics Engineers J.* 1959, **15**, 413.
13. Reich, S., Friesem, A. A. and Rav-Noy, Z. in *Applied Holography and Optical Data Processing, Proceedings of an International Conference* (Ed. E. Marom, A. A. Friesem and E. Wiener-Aunear), Pergamon, Oxford, 1974, pp. 371–379.
14. Pinsl, J., Deeg, F. W. and Bräuchle, C., *Appl. Phys.* 1986, **B40**, 77.
15. Kogelnik, H., *Bell Systems Technical J.* 1969, **48**, 2909.
16. Dachs, H. *Topics in Current Physics—Neutron Diffraction* Springer Verlag, Berlin, 1978.
17. Keichling, U. and Wiedenmann, A., *Physica B* 1995, **213–214**, 895.
18. Wegner, E. and Adamson, A., *J. Am. Chem. Soc.* 1966, **88**, 394.
19. Kutal, C., Grutsch, P. and Yang, D. B., *Macromolecules* 1991, **24**, 6872.
20. Sears, V. F. *Methods of Experimental Physics*, Vol. 23, Part A. Academic Press, New York, 1986.
21. Maconnachie, A., *Polymer* 1983, **25**, 1068.
22. Coyne, L. D. and Wu, Wen-Li, *Polym. Commun.* 1989, **30**, 312.